

# Theoretical and experimental studies of electrical conductivity for functionally graded, heterogeneous surfaces

Cite as: J. Appl. Phys. **125**, 035106 (2019); doi: [10.1063/1.5079556](https://doi.org/10.1063/1.5079556)

Submitted: 31 October 2018 · Accepted: 30 December 2018 ·

Published Online: 18 January 2019



J. M. Jennings,<sup>1,a)</sup>  R. Vaidyanathan,<sup>2</sup> and A. Kar<sup>3</sup> 

## AFFILIATIONS

<sup>1</sup>Materials Science and Engineering, University of Central Florida, Orlando, Florida 32816, USA

<sup>2</sup>Advanced Materials Processing and Analysis Center (AMPAC), Materials Science and Engineering, Mechanical and Aerospace Engineering, University of Central Florida, Orlando, Florida 32816, USA

<sup>3</sup>Laser-Advanced Materials Processing Laboratory, Center for Research and Education in Optics and Lasers (CREOL), College of Optics and Photonics, University of Central Florida, Orlando, Florida 32816, USA

<sup>a)</sup>Present address: The Harris Corporation, 1025 W. NASA Boulevard Melbourne, Florida 32919, USA. **Electronic mail:** [jjenni02@harris.com](mailto:jjenni02@harris.com)

## ABSTRACT

A theoretical approach for estimating solutions to Maxwell's equations for structures with spatially-varying electromagnetic properties is presented for conductive media containing surfaces modified with functionally graded, heterogeneous electrical conductivity. The basis of the approach is an equivalent depth technique that replaces a graded conductivity region consisting of a phase mixture with a series of thin layers with uniform, multi-phase properties locally matching the effective mixture properties of the graded region. Radio frequency field propagation within each layer is determined as if it had existed within a constant conductivity medium but its depth is electromagnetically equivalent to the replaced graded region existing prior to the layer. The equivalent depth approach was applied to planar, thin foil, and cylindrical media to enable comparison with experimental results. Model predictions were compared with total transmission results for Pt-doped titanium thin foils and steady-state temperature rise in closed wire loops made from Sn-modified copper wire. For the thin foil case, the model-predicted total transmissivity shows good agreement with trends in the experimental results due to property changes in the modified surface layers. In the cylindrical wire case, similar agreement between the predicted effective conductivity values for the modified layers and experimental results was observed. Thus, the equivalent depth approach is an effective method for estimating solutions to Maxwell's equations in complex media and a useful tool for predicting the performance of tailored surface conductivity modifications.

Published under license by AIP Publishing. <https://doi.org/10.1063/1.5079556>

## I. INTRODUCTION

Tailoring surface electromagnetic properties (conductivity and permeability) in conductors is a growing field of interest with a wide variety of potential applications where modifying a material's response to incident radio frequency (RF) fields is beneficial.<sup>1</sup> When time-varying RF fields impinge upon a dielectric-conductor interface, eddy currents are produced. The extent of RF field-to-induced current conversion at the interface depends upon the RF field's propagating

characteristics (wavelength, direction, etc.), the interface geometry, and the electromagnetic (EM) property differences at the boundary. Within the conductor, those currents remain concentrated near the surface due to the skin effect.<sup>2</sup> Surface tailoring takes advantage of this phenomenon by introducing surface and subsurface modifications to the conductor's EM properties to produce beneficial effects with minimal impact on the bulk material properties. Examples of potential applications for surface tailoring include reducing the induced current

and subsequent Joule heating that occurs in an implanted medical device lead during magnetic resonance imaging (MRI) and increasing the Joule heating within the thermosensing layer of a metal foil bolometer for enhanced sensitivity.<sup>3-5</sup>

The surface tailoring approach relies on the same processing techniques traditionally used to adjust a material's mechanical surface properties (wear, hardness, etc.) like modifications to a surface's chemical composition, microstructure, or geometry to alter its EM properties. The introduction of impurities, plastic deformation, and grain refinement all tend to decrease electrical conductivity while the introduction of additional material phases generally produces effective media property values within the Hashin and Shtrikman bounds.<sup>6-12</sup> The geometry of those included phases can also impact the modified properties achieved.<sup>13</sup> Advanced laser surface treatments and other traditional thermochemical processes are capable of producing surface layers with a variety of complex concentration profiles at depths comparable to the skin depth for a wide range of RF frequencies.<sup>3,14-17</sup>

A key step in implementing the EM surface property tailoring approach is developing techniques for predicting their performance in real world applications. This requires the incorporation of spatially-dependent electromagnetic surface properties into solutions of Maxwell's field equations for different interface configurations. This requirement matches those evaluations commonly practiced in the analysis of transport properties (e.g., heat flow, stress versus strain, etc.) through functionally graded materials (FGMs).<sup>18</sup> In the analysis of FGMs and other heterogeneous media, numerous analytical approaches for determining effective transport characteristics with similar linear constitutive relationships for materials with graded or non-uniform properties exist.<sup>12</sup> For example, Brandhari and Purohit utilized a depth-dependent, volume-fraction power law relationship to estimate modulus values in a layered numerical analysis evaluating the stress versus strain relationship occurring during transverse loading in planar FGMs.<sup>19</sup> Wu and Kuo applied a comparable method investigating bending stresses versus strains in layered cylindrical composite tubes.<sup>20</sup> Alternately, Duan *et al.* used a differential replacement procedure to determine the effective direct current (DC) electrical conduction through a heterogeneous medium containing graded transitions between the two-phase components.<sup>21</sup> Although these earlier works address elements associated with the modified EM property surface layer analysis, further advancement is required to apply these heterogeneous media and FGM concepts to time-varying RF fields.

The objective of the current work is to present an approach for estimating solutions to Maxwell's equations for an interface between a dielectric and a conductor with modified EM properties. Two interface geometries are considered where they have a broad range of applicability to real world situations, have existing constant property solutions, and can be evaluated experimentally. These cases, shown in Fig. 1, are (1) a semi-infinite thin foil with a modified conductivity layer exposed to an incident RF magnetic field parallel to the surface and (2) an infinite cylindrical conductor with a

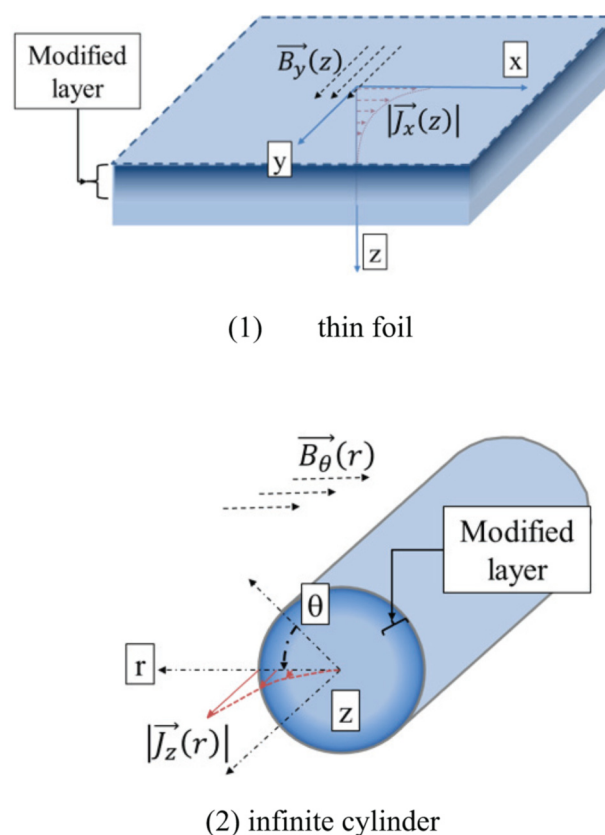


FIG. 1. Dielectric-to-conductor with modified EM property interfaces evaluated.

radially-dependent modified conductivity surface layer exposed to an external transverse RF magnetic field.

The derivation will introduce the equivalent depth concept and apply it to predict applicable RF field distributions within conductive media with spatially-dependent electrical conductivities. Those predictions are then compared with experimental results for validation. Measured transmissive properties of titanium foils doped with platinum via laser-assisted, chemical vapor deposition, and thermal diffusion produced by our research group (Chen *et al.*) in an earlier work are compared with predictions for the surface modified foil based on an assumed dopant distribution.<sup>14</sup> For the cylindrical case, modified surface specimens were produced from tin-plated, solid-round copper wire using heat treatment. When possible, microstructural analysis was utilized to characterize the modified layers and the effective conductivity values were predicted using the equivalent depth approach. Joule heating (steady-state temperature rise) during RF magnetic field exposure for the modified wires in a closed-loop configuration was compared with reference wire loops with uniform properties. The differences between the predicted effective conductivities and those determined using DC methods were also assessed.

## II. MODEL DERIVATION

### A. Equivalent depth approach

When the electrical conductivity value within a graded EM property region transitions continuously from a surface value to that of the core due to changes in depth-dependent composition of a multiphase mixture, it is assumed that the graded region can be subdivided into a sufficient number of narrow constant property segments,  $M$ , perpendicular to the grading coordinate. Within each segment,  $i$ , the constant conductivity value is taken as the average between the effective values at the entrance and exit of the given segment determined from the compositional makeup at each of those depths. The effective conductivity values at each of these locations can be determined using any effective medium model (e.g., Hashim and Shtrikman, Hamilton-Crosser, Landauer, etc.).<sup>7,12,13</sup> For simplicity, the derivation in the current study utilizes a volumetric rule-of-mixtures.<sup>19</sup> Within the graded region, the typical effective medium assumptions apply including: the modified layer responds as a multiphase continuum in the plane normal to the depth coordinate; the phases are randomly distributed within each depth plane; and the size scale of the pure constituent phases is small ( $<0.1\lambda$ ) compared to the propagating RF field wavelength,  $\lambda$ .<sup>12</sup> When analyzing the time-varying, induced current or field amplitude distribution versus depth across the segment, the governing equation with the segment's constant properties derived from Maxwell's equations is applied for the applicable coordinate system. However, the governing equation is applied to an adjusted depth coordinate unique to each segment which is determined by replacing all intervals prior to the one under analysis with the same effective property values with a depth electromagnetically equivalent to the graded region it replaces. This replacement approach is repeated for every segment in the graded region until the conductivity value converges to that for the core material where the remaining distribution calculated within the adjusted depth coordinate is determined within the last segment.

### B. Thin foil model

For the uniform surface modification of a planar medium, it is assumed that the modified effective conductivity value is linear and isotropically perpendicular to the surface and only changes as a function of depth,  $z$ . Insertion of this depth variability into Faraday's and Ampere's laws for a conductive medium in terms of the current density,  $\vec{J}$ , and magnetic flux density,  $\vec{B}$ , is shown in Eqs. (1) and (2), where  $\omega$  is the radial frequency;  $j$  is  $(-1)^{1/2}$ ; and  $\sigma(z)$  and  $\mu(z)$  are the depth dependent conductivity and permeability values, respectively,

$$\Delta \times ([\sigma(z)]^{-1}\vec{J}) = -j\omega\vec{B}, \quad (1)$$

$$\Delta \times [\mu(z)]^{-1}\vec{B} = \vec{J}. \quad (2)$$

Applying these equations to the modified planar thin foil interface in Fig. 1, the non-linear differential equation

describing the current density distribution's relationship with depth into the conductive medium becomes

$$J'_x(z) + b(z)J'_x(z) + [c_{RE}(z) - jc_{IM}(z)]J_x(z) = 0, \quad (3)$$

where

$$b(z) = \left[ \mu(z) \frac{\partial}{\partial z} [\mu(z)]^{-1} + 2\sigma(z) \frac{\partial}{\partial z} [\sigma(z)]^{-1} \right], \quad (4)$$

$$c_{RE}(z) = \sigma(z) \frac{\partial^2}{\partial z^2} [\sigma(z)]^{-1} + \mu(z) \frac{\partial}{\partial z} [\mu(z)]^{-1} \sigma(z) \frac{\partial}{\partial z} [\sigma(z)]^{-1}, \quad (5)$$

and

$$c_{IM}(z) = \omega[\sigma(z)\mu(z)]. \quad (6)$$

With the coefficients of the governing equation now in terms of the electromagnetic property variation with depth, a means of describing those variations within the graded EM property region with a continuous function is selected. The depth dependent effective property value of a planar two-phase mixture which transitions through the graded region of the substrate is calculated using the relationship shown in Eq. (7), where  $P_m(z)$  is the modified property value in a plane at a depth along the  $z$  axis;  $P_s$  is the property value for the pure surface addition;  $P_c$  is the property value of the core material; and  $V_f(z)$  is the volume fraction of the added phase at depth  $z$ .<sup>19</sup>

$$P_m(z) = (P_s - P_c)V_f(z) + P_c = \Delta P_{\max}V_f(z) + P_c. \quad (7)$$

Although any continuous function can be applied to model the volume fraction distribution,  $V_f(z)$ , a power law relationship is one that provides a fair degree of flexibility in its ability to match many of the monotonic distributions that are likely to be produced by typical surface treatment methods. In the planar case, this takes the form shown in Eq. (8), where  $z_M$  is the depth of the graded region,  $n$  is the exponent used for tuning the distribution shape, and  $h$  is the depth required to make a complete concentration transition from the pure surface addition's EM property value to that of the core

$$V_f(z) = \left( \frac{-z + z_M}{h} \right)^n. \quad (8)$$

In many cases,  $h$  will extend beyond the core material's surface and into a virtual region above the surface where a full phase-to-core transition would occur. In this case,  $h$  is related to the property value at the substrate's surface,  $P_{\text{surf}} = P_m(0)$  by

$$h = z_M \left( \frac{P_{\text{surf}} - P_c}{\Delta P_{\max}} \right)^{-1/n}. \quad (9)$$

How these FGM parameters relate to the interface is shown in Fig. 2. These parameters can either be optimized during a modified surface layer design or chosen to fit a volume fraction profile matching the observed element/phase distributions in fabricated articles as is the case in the current work.



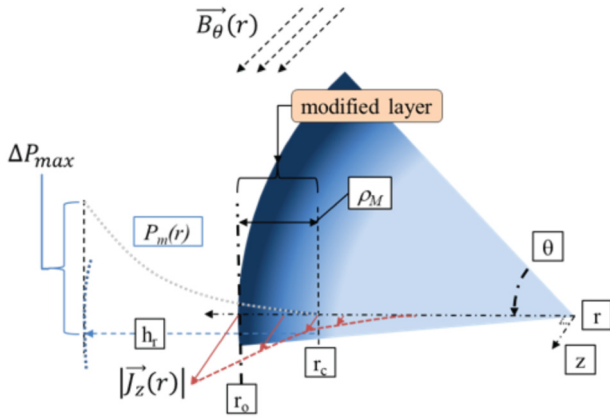


**FIG. 3.** Equivalent depth parameters associated with analysis of semi-infinite cylindrical conductive medium with modified surface electromagnetic properties exposed to transverse RF magnetic field.

frequency,  $\omega$ , and the volume fraction distribution parameters  $h_r$  and  $n$

$$J_z''(r) + \left(\frac{1}{r} - b_r(r)\right)J_z'(r) + [c_{RE,r}(r) - jc_{IM,r}(r)]J_z(r) = 0, \quad (17)$$

where  $b_r(r)$ ,  $c_{RE,r}(r)$ , and  $c_{IM,r}(r)$  are all functions of the pure EM properties of the base and added material phases,  $n$  and  $h_r$ . The equivalent depth approach is applied by dividing the modified layer into  $M$  constant property segments, which simplifies this governing equation within each segment  $i$  to the linear form shown in Eq. (18)

$$J_{z,i}''(r) + \left(\frac{1}{r}\right)J_{z,i}'(r) + [-jc_{IM,ave-r,i}]J_{z,i}(r) \approx 0, \quad (18)$$

where  $c_{IM,ave-r,i}$  is the average of the value of  $c_{IM,r}(r) = \omega[\sigma(r)\mu(r)]$  found at the depth  $(i-1)$  and  $i$  times the segment depth,  $\delta\rho$ , which is equal to  $r_o - r_c$  divided by  $M$  and  $J_{z,i}(r)$  is the current distribution in interval  $i$ . A solution to this governing equation found by applying the applicable EM wave boundary conditions for the cylinder (field continuity at the cylinder surface and field gradients converge to 0 as  $r \rightarrow 0$ ) is the ratio between the modified Bessel function of the first kind of the zeroth order,  $I_0[k_i(r_i)r]$  found at  $r$  and at the cylinder's surface radius,  $r_o$ , where  $k_i(r_i)$  is the value of the complex wave number equal to  $\sqrt{c_{IM,r,i}}$ .<sup>23</sup> The change in the current density value,  $\Delta J_{z,i}(r)$  within the segment,  $i$ , at an equivalent radius value,  $r_{eq}$ , is found utilizing Eq. (19), and the corresponding current value,  $J_{z,i}(r)$ , is found from Eq. (20)

$$\frac{\Delta J_{z,i}(r)}{J_{z,o}} \approx \frac{1}{I_0(k_i(r_{eq})r_{eq})} [I_0(k_i(r_i)r) - I_0(k_i(r_i)r_{i-1})], \quad (19)$$

$$\frac{J_{z,i}(r)}{J_{z,o}} = 1 - \frac{\Delta J_{z,i}(r)}{J_{z,o}} - \sum_{m=1}^{i-1} \frac{\Delta J_{z,m}(r_o - m\delta\rho)}{J_{z,o}}. \quad (20)$$

The value of  $r_{eq}$  is approximated from the current value calculated at the interior of the previous interval,  $i-1$ , using Eq. (21), where  $\rho_{eq}$  is the corresponding equivalent depth between the equivalent surface and  $r$

$$r_{eq}(r_i) = r + \rho_{eq}(r_i) \approx r + \text{Re} \left[ \sqrt{\frac{1}{jc_{IM,ave-r,i}}} \ln \left( \frac{J_z(r_{i-1})}{J_{z,o}} \right) \right]. \quad (21)$$

Beyond the modified layer, the current and field distributions are calculated using the equivalent radius value found at  $i=M$ . The effective wave number of the modified surface specimens,  $k_{eff}$ , and the corresponding effective conductivity,  $\sigma_{eff}$ , are determined at the  $r$  value when the current density ratio  $J_z(r)/J_z(r_{eq})$  equals  $1/e$ .

### III. EXPERIMENTAL METHODS

For validation of the proposed depth equivalent modeling approach, samples with modified conductivity layers matching the analyzed configurations were fabricated and their RF field interactions measured for comparison with model predictions. For the thin foil model, experimental results documented by Chen *et al.* for modified thin (25 and 50  $\mu\text{m}$ ) titanium foils doped with platinum were used.<sup>14,15</sup> The Pt concentrations within the EM property modified layer were determined using electron dispersive X-ray spectroscopy (EDS) of the doped surfaces. The transmissive properties of the foils were assessed by comparison between the magnetic field strength measured between two Hewlett Packard 11940 close field magnetic probes placed in close proximity with and without foils present in the configuration shown in Fig. 4.<sup>14</sup> The transmitted field was produced using a signal generator to supply a 63.86 MHz sinusoidal signal to the transmit probe and the receiver probe output was recorded using a spectrum analyzer. During transmission measurements, the foils were sandwiched between thick brass plates with matching apertures in order to attenuate the fields' outboard of the foil sample preventing them from affecting the measured results.

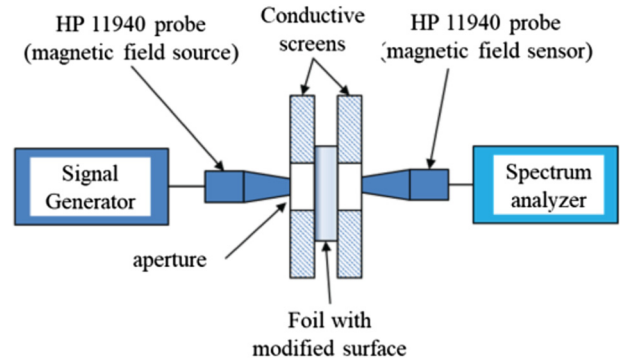


**FIG. 4.** Schematic view of thin foil experimental setup used by Chen *et al.* (Ref. 14).

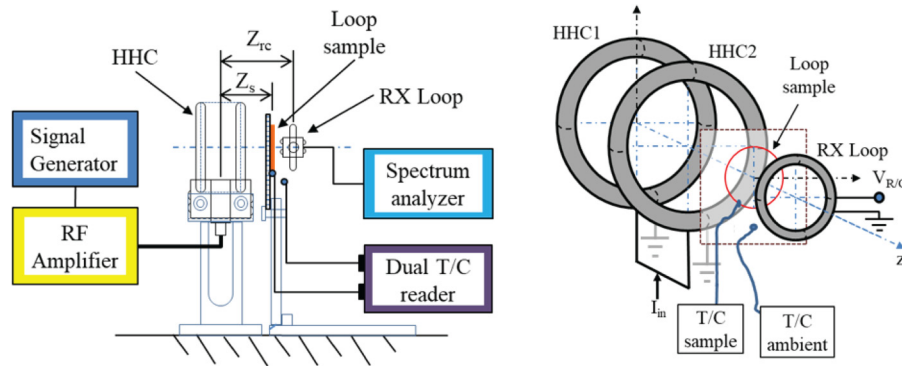


FIG. 5. Schematic view of closed loop experimental setup by Jennings *et al.* (Refs. 24 and 25).

For the assessment of the cylindrical model, EM property modified layers were formed on AWG 26-gauge tin-plated copper wire. Wire sections were coated with ceramic mold release to inhibit oxidation and heat treated in a  $\sim 470^\circ\text{C}$  furnace in air for various times to alter the extent of Sn-Cu diffusion. Upon removal from the furnace, the wire segments were immediately quenched in an ambient water bath. The properties of the Sn-Cu layers formed were then determined using EDS line scans of wire cross sections using a Hitachi S-3700N variable pressure (VP) scanning electron microscope (SEM) at 15 keV with a Bruker X-flash silicon-based EDS. Model validation was achieved using Joule heating comparisons between these Sn-modified Cu wires and those with uniform EM properties. The reference materials, pure copper, 100 aluminum, 260 brass, and 300-series stainless steel, were selected because they each have a relative permeability near 1.0 and spanned a conductivity range from  $\sim 6$  to  $0.1 \times 10^7$  ( $\Omega\text{m}$ ) $^{-1}$  which bound the range expected for any Sn-Cu mixture.

Steady-state temperature rise for circular closed wire loops exposed to sinusoidal RF magnetic field was measured using the test configuration shown in Fig. 5. Details associated with the testing and analysis of the data are included in Refs. 24 and 25.

The sample is placed within a coaxial loop array between a transmitting Helmholtz coil (HHC) and a receiving loop antenna used to monitor the field strength throughout the duration of the experiment. The HHC is driven using an amplified signal generator producing a  $\sim 42$  dBm continuous-wave, sinusoidal signal which results in a magnetic flux density at the loop near  $\sim 14\ \mu\text{T}$  matching the RF magnetic field strength for a typical 1.5 T MRI system.<sup>4</sup> The thermocouple (T/C) outputs are displayed on a digital thermal couple reader with  $0.1^\circ\text{C}$  resolution and  $+0.1\% + 0.6^\circ\text{C}$  accuracy. For comparison with the RF test results, DC conductivity values for the wires were also determined by calculating the conductivity from experimentally determined DC resistance through  $\sim 100$  mm wire spans using a micro-ohmmeter.

## IV. RESULTS AND DISCUSSIONS

### A. Thin foil, comparison with actual surface modified materials

A summary of the processing conditions and experimental results determined by Chen *et al.* for the different Pt-doped Ti foils formed, including the measured transmissivity ratio,  $t_{e\text{-tot}}$ , are included in Table I.

TABLE I. Sample description and experimental results for experiments by Chen *et al.*<sup>15</sup>

Thickness ( $\mu\text{m}$ )	Sample name	Laser interaction time (s)	Estimated peak processing temperature ( $^\circ\text{C}$ )	Pt surface concentration ( $\times 10^{-4}$ )	$t_{e\text{-tot}}$ ( $\times 10^{-5}$ )
25	As received	N/A	N/A	N/A	$1.463 \pm 0.024$
	Az6	0.333	1414	7.92	$1.148 \pm 0.025$
	Lperp6	0.333	1388	7.50	$1.128 \pm 0.025$
	Az12	0.167	926	3.08	$1.229 \pm 0.076$
	Lperp12	0.167	947	2.10	$1.266 \pm 0.025$
	As received	N/A	N/A	N/A	$0.368 \pm 0.013$
50	Az6	0.333	1194	8.19	$0.322 \pm 0.013$
	Lperp6	0.333	1170	9.89	$0.316 \pm 0.013$
	Az12	0.167	767	3.29	$0.343 \pm 0.013$
	Lperp12	0.167	781	1.54	$0.341 \pm 0.013$

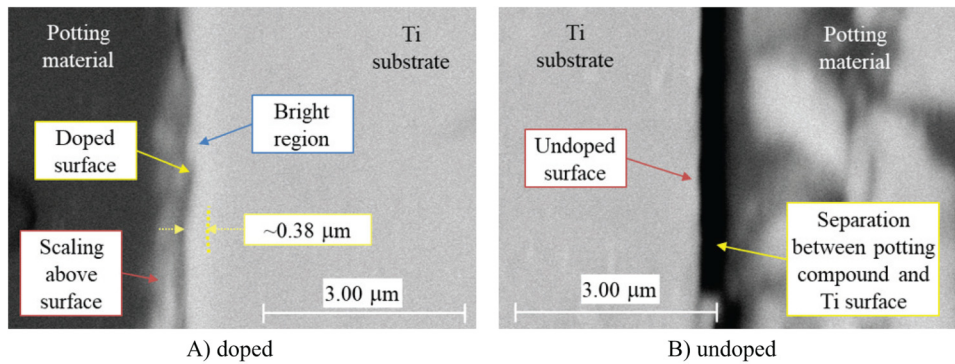


FIG. 6. Backscatter SEM image of (A) Pt-doped and (B) undoped Ti surfaces.

Typical backscatter SEM images of cross sectioned Ti foils with and without a modified region are shown in Fig. 6. A slightly brighter region adjacent to the doped surface indicates the higher concentration of higher density Pt in the modified region not observed in undoped locations. Evidence of “scaling” is also seen above the surface which likely formed during the rapid cool-down that occurs following laser irradiation.

Because the modified layer depth approached the detectability thresholds for SEM/EDS characterization, it was necessary to estimate analytically the Pt concentration profile in the graded region. The concentration profiles were assumed to match that for a one-dimensional instantaneous source, non-steady-state solution for a semi-infinite plane shown in Eq. (22)

$$c(z, t) = c_0 + c_0 \operatorname{erf}\left(\frac{z}{\sqrt{4D(T)t}}\right), \quad (22)$$

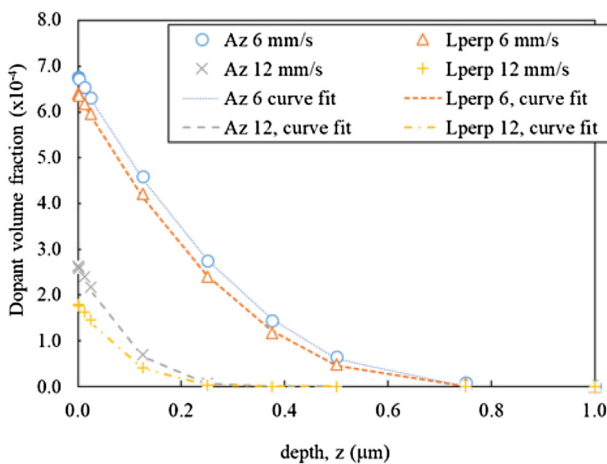


FIG. 7.  $V_f$  curve fit and estimated Pt dopant distribution in the Ti foil versus depth: based on EDS results for surface Pt concentration—25  $\mu\text{m}$  thick.

where  $c_0$  is the initial surface concentration of dopant deposited assumed to be equal to the EDS determined surface concentration;  $t$  is time assumed to match the laser interaction time for the particular scanning rate used during processing;  $T$  is the peak surface processing temperature achieved during the total duration of the interaction time temperature; and  $D(T)$  is the temperature dependent diffusivity of Pt in Ti found using Eq. (23) from available diffusion-related values for Pt and Ti in the literature, where  $D_0$  is assumed to be  $7.6 \times 10^{-6} \text{ cm}^2/\text{s}$ ;  $Q_b$  is 121 kJ/mol; and  $R$  is Boltzmann’s constant equal to 8.31446 J/(mol K)<sup>26,27</sup>

$$D(T) = D_0 e^{-Q_b/RT}. \quad (23)$$

These estimated concentration gradients are converted to volume fraction and the power law parameters,  $n$  and  $z_M$ , from Eq. (8) were selected. The resultant volume fractions

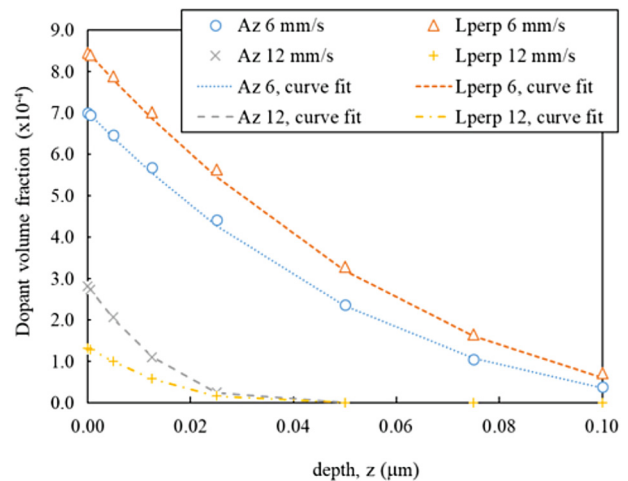


FIG. 8.  $V_f$  curve fit and estimated Pt dopant distribution in the Ti foil versus depth: based on EDS results for surface Pt concentration—50  $\mu\text{m}$  thick.

**TABLE II.** Summary of model  $V_f$  curve fit parameters that match estimated  $V_f$  distributions in the thin foil specimens.

Sample	25 $\mu\text{m}$ foil thickness		50 $\mu\text{m}$ foil thickness	
	$z_M$ ( $\mu\text{m}$ )	$n$	$z_M$ ( $\mu\text{m}$ )	$n$
Az6	0.75	2.2	0.15	2.7
Lperp 6	0.75	2.4	0.15	2.4
Az 12	0.375	3.4	0.04	2.5
Lperp 12	0.375	3.75	0.04	2.2

versus depth through the foils are shown in Figs. 7 and 8 and the resultant curve fit parameters for each case can be found in Table II.

Equivalent depth predictions of the transmissivity,  $t_{m-tot}$ , were compared with experimentally acquired results for  $t_{e-tot}$ . Pure constituent conductivity values of  $2.38 \times 10^6$  ( $\Omega\text{m}$ )<sup>-1</sup> and  $9.26 \times 10^6$  ( $\Omega\text{m}$ )<sup>-1</sup> were assumed for titanium and platinum, respectively, and both are assumed to have relative permeability values of 1.0.<sup>14</sup> A segment count of 100 which divided the graded regions into constant property regions with  $\delta z$  thickness values ranging from 0.00375 to 0.0075  $\mu\text{m}$  was chosen for the analysis.

The predicted values for  $t_{m-tot}$  are found to be of a similar order of magnitude as the measured results, near  $10^{-5}$ ; however, the relative changes between each case appear muted. This is most likely caused by the over-simplification of the RF magnetic field-thin foil interactions model which assumes the foil is semi-infinite in-plane, and the RF magnetic field is only parallel to the foil surface which does not completely capture the more complex configuration of the fields emitted from the transmitting probe. However, when the differences caused by each doping case,  $\Delta t_{tot}$ , are normalized by the full range and centered around the mean,

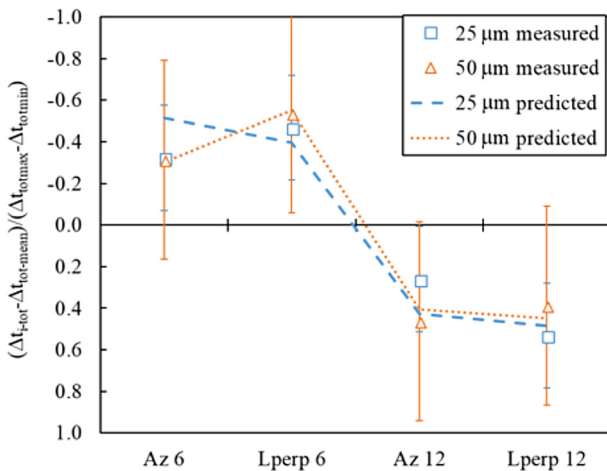


**FIG. 9.** Comparison of range normalized change in transmissivity from mean  $\Delta t_{i-tot}$  for doped and undoped foil samples.

**TABLE III.** Cylindrical circular, closed-loop sample descriptions, dimensions, and heat treatment conditions for wire materials evaluated.

Sample group	Sample name	Wire diameter (mm)	Average loop radius (mm)	Heat treatment: time (min)/temp ( $^{\circ}\text{C}$ )
Pure metal	Thick Cu 1	0.509	28.98	None
	Thick Al 1	0.494	28.98	None
	Thick brass 1	0.507	28.89	None
	Thick S.S. 1	0.495	28.95	None
Surface modified	H-C	0.508	28.91	None
	H-1	0.504	28.85	5/470 coated
	H-8	0.508	28.74	5/473 not coated
	H-5	0.505	28.79	90/477 coated

$\Delta t_{tot-mean}$ , the change trends predicted by the model closely match those of the experimental results for both foil thicknesses shown in Fig. 9.

### B. Cylindrical, comparison with actual surface modified materials

The heat treatment times for the modified wires and the resultant wire and loop radii for the circular closed loop samples tested are listed in Table III.

Backscatter SEM images showing the line scan locations for the microsectioned Sn-modified Cu wires are shown in Fig. 10. The unaltered case, sample H-C, shown in Fig. 10(a), reveals a nominal Sn plating thickness near 1–3  $\mu\text{m}$  and a relatively refined grain structure within the Cu bulk. For the five-minute heat-treated samples, H-1 (coated) and H-8 (uncoated) in Figs. 10(b) and 10(d) show Sn-rich phase islands on the surface of a 3–5  $\mu\text{m}$  thick Cu-Sn continuous layer with a thinner Cu-rich transition region into the bulk. The Sn-rich islands appear less populous in the uncoated case. In the 90-min heat-treated wire, shown in Fig. 10(c), a continuous 6–8  $\mu\text{m}$  thick Cu-Sn layer with no Sn-rich regions is observed. Any oxides formed on the surface during heat-treatment appear to have been removed during the mechanical removal of the mold release. The line scan results for the modified samples converted to volume fraction of Sn with respect to depth from the surface of the wire are shown in Fig. 11 and the corresponding curve fit parameters are shown in Table IV.

Because H-C contains a region of pure tin prior to the graded transition, an additional offset term that accounts for the constant property outer layer thickness is incorporated in the equivalent depth model,  $\rho_o$ . In the calculations of the two-phase effective property values, pure constituent conductivity values of  $5.88 \times 10^7$  ( $\Omega\text{m}$ )<sup>-1</sup> and  $0.870 \times 10^7$  ( $\Omega\text{m}$ )<sup>-1</sup> were assumed for Cu and Sn, respectively, and both are assumed to have relative permeability values of 1.0. The equivalent depth predictions were determined using a segment count of 100, which divided the graded regions into constant property regions with thicknesses,  $\delta\rho$  of approximately 0.03–0.14  $\mu\text{m}$ .

Table V contains the measured steady state temperature rise,  $\Delta T$ , and average magnetic flux recorded during each test.<sup>25</sup> Also included are the measured DC conductivity values

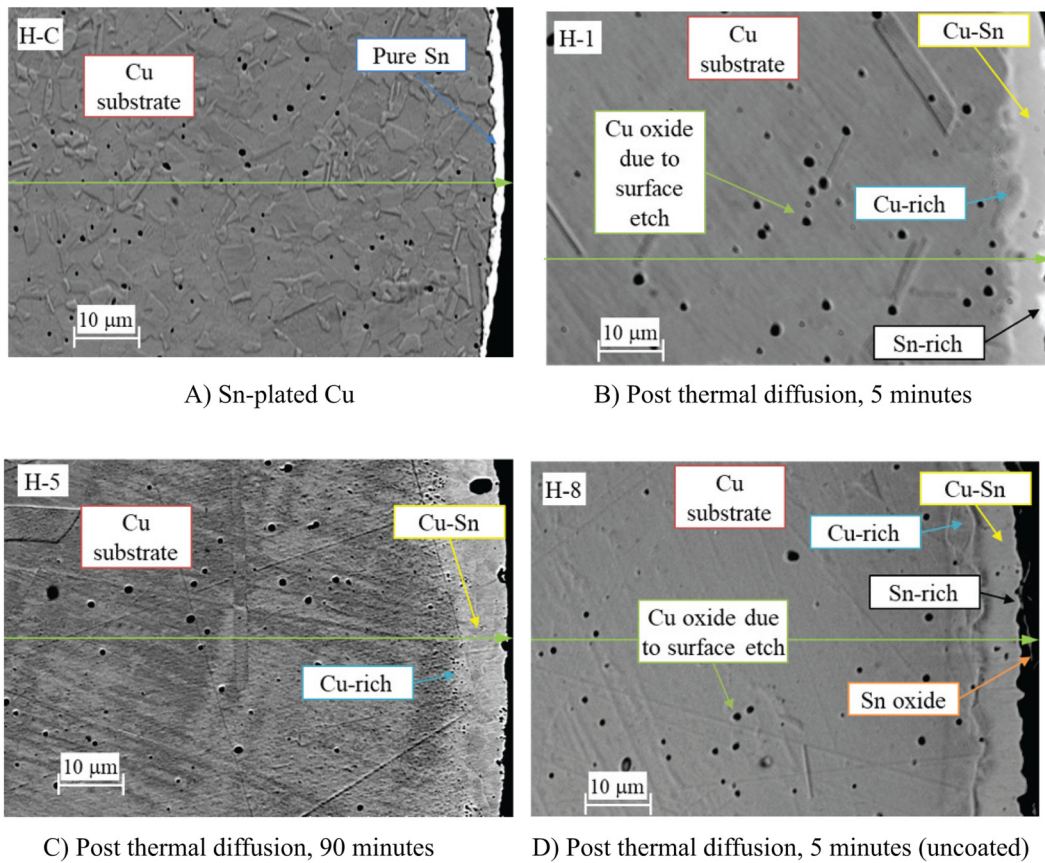


FIG. 10. Backscatter SEM micrographs of Sn-plated Cu wire before and after heat treatment. Bright region caused by higher density of Sn-rich phase.

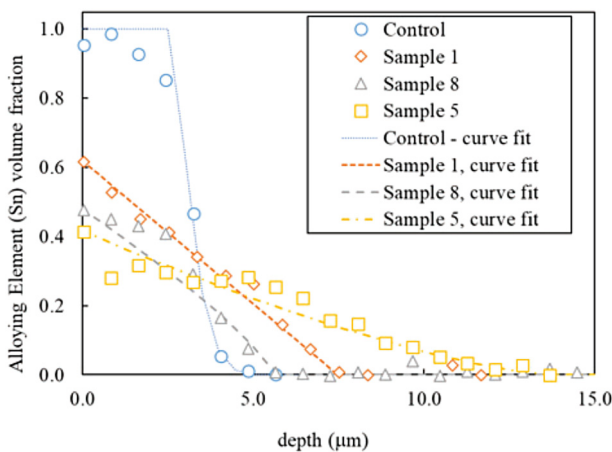


FIG. 11. EDS line scan-based volume fraction results for heat treated Sn-Cu wires along with corresponding volume fraction curve fits.

for each wire type and the effective values predicted for the Sn-modified Cu wires by the equivalent depth model. When compared with available conductivity data for the Cu-Sn binary system, this range of conductivity values indicates that the phases present within the modified layers formed are most likely graded, heterogeneous mixtures of  $\alpha$ -Cu and a Cu-rich Cu-Sn intermetallic.<sup>29</sup> The temperature rise results presented exhibit high variability. There are two primary sources for this variability. One is the difference in flux density applied during the steady state temperature rise

TABLE IV. Summary of model  $V_f$  curve fit parameters that match EDS results for modified wire samples.

Sample name	Outer plating layer, $\rho_o$ ( $\mu\text{m}$ )	$\rho_m = r_{\text{wire}} - r_c$ ( $\mu\text{m}$ )	$n$
H-C	2.75	2.998	5.0
H-1	0.0	7.480	1.0
H-8	0.0	5.618	0.8
H-5	0.0	13.742	1.4

TABLE V. Summary of experimental measurements and derived values for cylindrical sample steady state temperature testing.

Sample group	Sample name	Measured DC conductivity ( $\times 10^7$ 1/ $\Omega$ m)	Predicted effective conductivity ( $\times 10^7$ 1/ $\Omega$ m)	Average magnetic flux, $ B_{gs} $ ( $\mu$ T)	Measured temperature rise, $\Delta T$ ( $^{\circ}$ C)
Pure metal	Thick Cu 1	5.69		$11.57 \pm 0.05$	$0.5 \pm 0.1$
	Thick Al 1	3.40		$11.54 \pm 0.12$	$0.9 \pm 0.4$
	Thick brass 1	1.57		$11.46 \pm 0.07$	$0.9 \pm 0.1$
	Thick S.S. 1	0.14		$11.44 \pm 0.01$	$1.9 \pm 0.2$
Surface modified	H-C	5.74	2.99	$11.56 \pm 0.02$	$0.7 \pm 0.1$
	H-1	5.60	3.65	$11.50 \pm 0.11$	$0.5 \pm 0.1$
	H-8	5.32	4.10	$11.38 \pm 0.08$	$0.6 \pm 0.3$
	H-5	5.57	3.95	$11.26 \pm 0.03$	$1.1 \pm 0.4$

measurements. To normalize this effect, the temperature results plotted versus wire conductivity in Fig. 12 are divided by the square of the average applied magnetic field strength during the measurement. The other is the effectiveness of the thermocouple to accurately detect the surface temperature on the wire samples. The relative size of thermocouple tip to wire sample diameter and differences in thermal resistance through the thermal paste layer applied between them both affected these results. Despite the high variability, the trend observed for the reference samples clearly indicates the temperature rise varying inversely with the conductivity of the wire consistent with previous predicted results presented by Barletta and Zanchini.<sup>28</sup>

Plotting the modified wire normalized  $\Delta T$  results versus their DC conductivity values (where all were similar to Cu) shows an average curve offset from the reference curve. On the other hand, when the modified results are plotted versus their equivalent depth predicted effective conductivity values, the trend line agrees closely with the reference curve. This agreement reflects the effectiveness of the equivalent depth

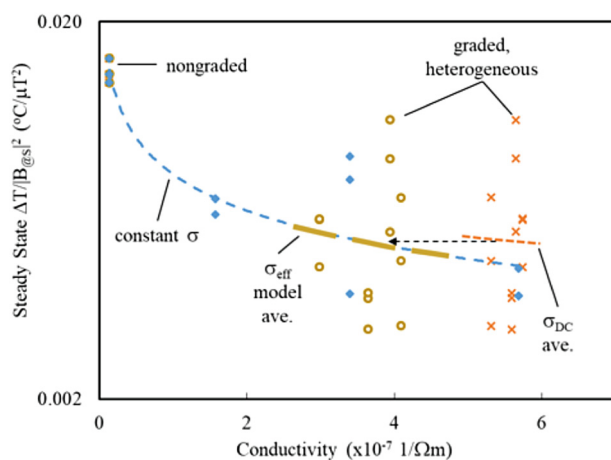


FIG. 12. Flux normalized steady state  $\Delta T$  versus conductivity for circular closed loop wire samples.

approach in determining the effective surface properties of wire.

## V. SUMMARY

In this work, the derivation of semi-analytical methods for determining the induced current distribution within planar, thin foil, and cylindrical media modified with surface layers containing graded, heterogeneous electrical conductivity values is presented. Experiments were conducted on surface modified materials in these configurations and their results were compared with those predicted by the models: transmissivity through Pt-doped titanium foils in the planar case; and temperature rise in Sn-modified, round copper wire closed loop samples exposed to an RF magnetic field for the cylindrical model case. Based on those results, the following can be concluded:

1. The thin foil model of the Pt-doped titanium transmissivity effectively predicts the trending caused by variations within the thin foil experimental results; however, the initially derived model was oversimplified when compared with the experimental configuration.

2. The transmissivity results were dominated by the surface properties, and the extremely thin Pt doping layers caused only a minor effect due to the limited surface modification applied; thus, there is likely a lower threshold where the need to account for the graded layer would not be required.

3. The equivalent length cylindrical model effectively predicts trends in steady state temperature rise for the Sn-modified closed-loop Cu samples in an inductive RF magnetic field environment; however, high variability in the temperature rise results did cloud the quality of the results.

4. The planar two-phase mixing assumption for property determination within the graded, heterogeneous region was the effect for determining the properties within both the Pt-doped titanium and Sn-modified Cu material cases.

5. Further work is required to improve the precision and accuracy of temperature rise within the wire samples subjected to this type of induction-based Joule heating experiment. Also, the effects of frequency and effective medium models on the equivalent depth approach's effectiveness in estimating solutions to Maxwell's equations with spatially dependent properties require further study.

## REFERENCES

- <sup>1</sup>A. Kar and R. Vaidyanathan, "Surface modified materials for tailoring responses to electromagnetic fields," U.S. patent 0296350, A1 (22 November 2012).
- <sup>2</sup>J. A. Stratton, *Electromagnetic Theory* (McGraw-Hill Book Company, Inc., New York, 1941), pp. 490–524.
- <sup>3</sup>O. Benafan, S.-Y. Chen, A. Kar, and R. Vaidyanathan, *Rev. Sci. Instrum.* **86**, 123903-1 (2015).
- <sup>4</sup>J. Nyenhuis, "MRI interactions with medical implants," in *IEEE International Symposium on Electromagnetic Compatibility*, Minneapolis, MN (IEEE, 2002).
- <sup>5</sup>A. Fantom, *Radio Frequency and Microwave Power Measurements* (Peter Peregrinus Ltd., London, 1990), pp. 72–98.

- <sup>6</sup>Z. Hashin and S. Shtrikman, *J. Appl. Phys.* **33**, 3125 (1962).
- <sup>7</sup>R. Landauer, *J. Appl. Phys.* **23**, 779 (1952).
- <sup>8</sup>C. Ho, M. W. Ackerman, K. Y. Wu, T. N. Havill, R. H. Bogaard, R. A. Matula, S. G. Oh, and H. M. James, *J. Phys. Chem. Ref. Data* **12**, 183 (1983).
- <sup>9</sup>R. Dannenberg and A. H. King, *J. Appl. Phys.* **88**, 2623 (2000).
- <sup>10</sup>A. S. Karolik and A. A. Luhvich, *J. Phys. Condens. Matter* **6**, 873 (1994).
- <sup>11</sup>K. M. Mannan and K. R. Karim, *J. Phys. Metal Phys.* **5**, 1687 (1975).
- <sup>12</sup>M. Wang and N. Pan, *Mater. Sci. Eng. R* **63**, 1 (2008).
- <sup>13</sup>R. L. Hamilton and O. K. Crosser, *Ind. Eng. Chem. Fundamentals* **1**, 187 (1962).
- <sup>14</sup>S. Y. Chen, O. Benafan, R. Vaidyanathan, and A. Kar, *Opt. Laser Eng.* **62**, 132 (2014).
- <sup>15</sup>S.-Y. Chen, O. Benafan, R. Vaidyanathan, and A. Kar, *Appl. Phys. A Mater. Sci. Process.* **116**, 703 (2014).
- <sup>16</sup>Y. J. Won and H. Ki, *J. Appl. Phys.* **113**, 174910-1 (2013).
- <sup>17</sup>W. M. Steen, *Laser Material Processing*, 3rd ed. (Springer-Verlag, London, 2003), pp. 227–228.
- <sup>18</sup>M. Naebe and K. Shirvanimoghaddam, *Appl. Mater. Today* **5**, 223 (2016).
- <sup>19</sup>M. Brandari and K. Purohit, *IOSR J. Mech. Civil Eng.* **10**, 46 (2014).
- <sup>20</sup>C. P. Wu and C.-H. Kuo, *Appl. Math. Model.* **37**, 916 (2013).
- <sup>21</sup>H. L. Duan, B. L. Karihaloo, and J. Wang, *J. Appl. Phys.* **100**, 034906-1 (2006).
- <sup>22</sup>Z. Popovic and B. D. Popovic, *Introductory Electromagnetics* (Prentice Hall, Upper Saddle River, New Jersey, 2000), pp. 383–385.
- <sup>23</sup>P. A. Bottomly and E. R. Andrew, *Phys. Med. Biol.* **23**, 630 (1978).
- <sup>24</sup>J. M. Jennings, R. Vaidyanathan, and A. Kar, “Uncooled resistive metal foil bolometers for imaging with radiofrequency magnetic fields,” in *Image Sensing Technologies: Materials, Devices, Systems, and Applications V*, SPIE Conference, Orlando, FL (SPIE, 2018).
- <sup>25</sup>J. M. Jennings, A. Kar, and R. Vaidyanathan, “Induced current determination in MRI-like conditions using near field antenna interactions,” *Rev. Sci. Instrum.* (unpublished).
- <sup>26</sup>R. W. Balluffi, S. M. Allen, and W. C. Carter, *Kinetics of Materials* (John Wiley & Sons, Inc., Hoboken, New Jersey, 2005), p. 105.
- <sup>27</sup>M. DiBattista and J. W. Schwank, *J. Appl. Phys.* **86**, 4902 (1999).
- <sup>28</sup>A. Barletta and E. Zanchini, *Wärme - und Stoffübertragung* **29**, 285 (1994).
- <sup>29</sup>R. J. Fields and S. R. Low, “Physical and mechanical properties of intermetallic compounds commonly found in solder joints,” in *Metal Science and Joining, Proceedings of TMS Symposium*, Cincinnati (TMS, 1991).